

# SCIENTIFIC REPORTS



OPEN

## Dipole orientation analysis without optical simulation: application to thermally activated delayed fluorescence emitters doped in host matrix

Takeshi Komino<sup>1,2,3</sup>, Yuji Oki<sup>3,4</sup> & Chihaya Adachi<sup>1,2,3,5</sup>

The dipole orientation of guest emitters doped into host matrices is usually investigated by angular dependent photoluminescence (PL) measurements, which acquire an out-of-plane PL radiation pattern of the guest-host thin films. The PL radiation patterns generated by these methods are typically analysed by optical simulations, which require expertise to perform and interpret in the simulation. In this paper, we developed a method to calculate an orientational order parameter  $S$  without the use of full optical simulations. The PL radiation pattern showed a peak intensity ( $I_{sp}$ ) in the emission direction tilted by  $40^\circ$ – $60^\circ$  from the normal of the thin film surface plane, indicating an inherent dipole orientation of the emitter. Thus, we directly correlated  $I_{sp}$  with  $S$ . The  $S - I_{sp}$  relation was found to depend on the film thickness ( $d$ ) and refractive indices of the substrate ( $n_{sub}$ ) and the organic thin film ( $n_{org}$ ). Hence,  $S$  can be simply calculated with information of  $I_{sp}$ ,  $d$ ,  $n_{sub}$  and  $n_{org}$ . We applied our method to thermally activated delayed fluorescence materials, which are known to be highly efficient electroluminescence emitters. We evaluated  $S$  and found that the error of this method, compared with an optical simulation, was less than 0.05.

In the last decade, research into organic light-emitting diodes (OLEDs) has developed remarkably, supported by advances in control over molecular dipole orientation in amorphous films<sup>1</sup>. In thin glassy films used as OLED materials dipoles horizontally oriented to the substrate surface can greatly improve device performance by increasing the outcoupling efficiency of electroluminescence (EL)<sup>2–4</sup>. Light-emitting layers are generally guest-host binary molecular systems, hence control is needed over the orientation of the emissive dye (guest molecule) embedded into the host matrix. Some recent studies have demonstrated an outstanding external EL quantum efficiency (EQE) of over 30% by engineering a horizontal dipole orientation of thermally activated delayed fluorescence (TADF) emitters<sup>5–7</sup>. This class of emitters can harvest triplet excitons to attain high EQE values equivalent to those of phosphorescence emitters<sup>8–10</sup>. Angular dependent photoluminescence (PL) measurements, developed by Brütting and co-workers, are the most effective method of assessing dipole orientation in thin films<sup>2–4</sup>. This method can be used to measure the out-of-plane PL intensity distribution of guest-host thin films, hereafter referred to as a radiation pattern. The radiation pattern is analysed by simulating the pattern that would result from various dipole orientations. Thus, one can determine the dipole orientation that reproduces the experimentally obtained radiation pattern. The dipole orientation is a fundamental property of glassy and soft organic materials which governs their photonic, electronic, excitonic, and optical characteristics; hence this method is applicable not only to OLEDs but many other research fields. However, this method requires expertise

<sup>1</sup>Education Center for Global Leaders in Molecular System for Devices, Kyushu University, 744 Motooka, Nishi, Fukuoka, 819-0395, Japan. <sup>2</sup>Center for Organic Photonics and Electronics Research (OPERA), Kyushu University, 744 Motooka, Nishi, Fukuoka, 819-0395, Japan. <sup>3</sup>Japan Science and Technology Agency, ERATO, Adachi Molecular Exciton Engineering Project, 744 Motooka, Nishi, Fukuoka, 819-0395, Japan. <sup>4</sup>Department of Electronics, Kyushu University, 744 Motooka, Nishi, Fukuoka, 819-0395, Japan. <sup>5</sup>International Institute for Carbon Neutral Energy Research (WPI-I2CNER), Kyushu University, 744 Motooka, Nishi, Fukuoka, 819-0395, Japan. Correspondence and requests for materials should be addressed to C.A. (email: [adachi@cstf.kyushu-u.ac.jp](mailto:adachi@cstf.kyushu-u.ac.jp))

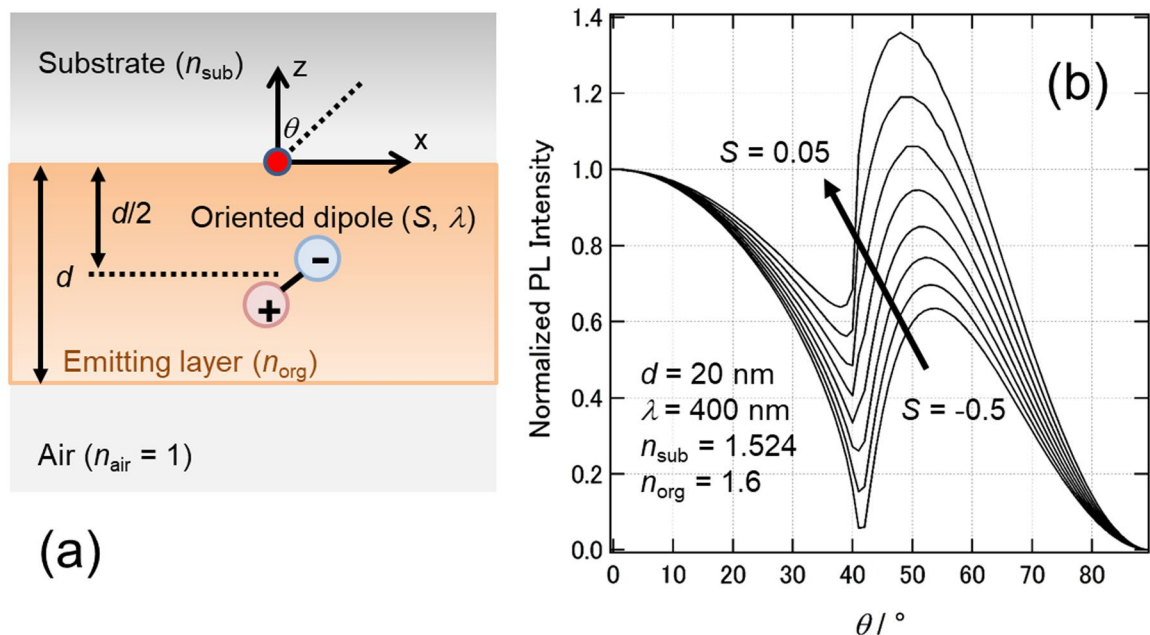


**Figure 1.** (a) Schematic model of the photonic mode simulation. (b) Simulation result for  $d = 20$  nm,  $\lambda = 400$  nm,  $n_{\text{sub}} = 1.524$ , and  $n_{\text{org}} = 1.6$ .

in optical simulation to analyse the radiation patterns and not all researchers are able to easily determine dipole orientations. A simple relation that directly connects the radiation pattern to the dipole orientation would enable more ready evaluation of dipole orientations without full optical simulations. This would allow wider uptake and application of this useful technique.

To date, four expressions have been proposed to define dipole orientation as follows. (i) The ratio of  $p_x$ ,  $p_y$ , and  $p_z$ , where  $p$  is the existence probability of a dipole<sup>2</sup>. The subscripts x, y, and z denote the direction of Cartesian coordinates where x and y are parallel to the substrate plane and z is orthogonal to the x-y plane. For a uniaxial dipole orientation,  $p_x = p_y \neq p_z$ . (ii) The ratio of vertically oriented dipoles versus the total dipoles is given by  $\Theta_v = p_z / (p_x + p_y + p_z)$ <sup>11</sup>. The dipoles are also occasionally substituted by the radiation power in this relation<sup>12</sup>. (iii) The ratio of horizontally oriented dipoles versus the total dipole is given by  $\Theta_h = (p_x + p_y) / (p_x + p_y + p_z)$ <sup>6,13</sup>. (iv) An orientational order parameter can be calculated as  $S = (p_z^2 - p_x^2) / (p_z^2 + 2p_x^2)$ <sup>14</sup>. Any of these parameters may be arbitrarily selected for analysis of the dipole orientation. In our previous studies, we have selected  $S$  for two reasons. First,  $S$  can express the uniaxial orientational order considering the distribution of dipole orientations in a system (e.g., crystals or glasses). Second,  $S$  values in guest-host systems can be compared with those in neat films; molecular orientations in neat films have been evaluated by  $S$ , so far. Note that  $S$  is defined as the order parameter for the emission ability ( $p_z^2$  and  $p_x^2$ ) here, rather than that for the molecular dipoles themselves ( $p_z$  and  $p_x$ ). In this paper, we sought a relation, to directly connect experimentally obtained radiation patterns with  $S$ . We found that  $S$  can be directly determined from the second peak intensity in the radiation pattern without the use of a full optical simulation.

## Results

First, we briefly describe the experimental method used to acquire radiation patterns. A detailed procedure is described elsewhere<sup>14</sup>. An approximately 15-nm-thick guest-host film is deposited on a transparent substrate (e.g., non-fluorescent glass or fused silica) and then encapsulated with a cover slip. Use of such an ultra-thin film enables us to assume the uniform exciton generation by photoexcitation, resulting in the simple optical model for the analysis. The substrate is attached to the flat plane of a fused silica half cylinder prism with matching oil having a refractive index close to that of the substrate. The thin film sample is subjected to an excitation light beam and the photoluminescence intensity in transverse magnetic (TM) mode is detected radially from the half cylinder prism. The radiation pattern is obtained by plotting the monochromatic PL intensity as a function of angle (emission angle,  $\theta$ ) between the normal of the substrate ( $\theta = 0^\circ$ ) and the emission direction in the x-z plane.

To determine a connection between the radiation pattern and  $S$ , we performed an optical simulation. A schematic model of the optical simulation is depicted in Fig. 1a. We set  $S_{\text{sim}}$  as the main variable, where the subscript “sim” indicates that the value was obtained by simulation. The radiation patterns were compared with simulated results with various values of  $S_{\text{sim}}$ . Figure 1b shows an example of the resulting radiation pattern when  $d = 20$  nm,  $\lambda = 400$  nm,  $n_{\text{sub}} = 1.524$ , and  $n_{\text{org}} = 1.6$  were used (light intensity was normalized at  $0^\circ$ ). These curves closely matched the experimentally obtained radiation patterns. We aimed to identify any special features of the curves that directly correlated with  $S$ . Looking at trends of the curves, we recognized that the second peak intensity ( $I_{\text{sp}}$ ) at  $40^\circ$ – $60^\circ$  monotonically increased as  $S_{\text{sim}}$  increased. Accordingly, we selected  $I_{\text{sp}}$  as a parameter to characterize the curves, where the parameters governing  $S_{\text{sim}}$  are  $I_{\text{sp}}$ ,  $d$ ,  $\lambda$ ,  $n_{\text{sub}}$ ,  $n_{\text{air}}$  and  $n_{\text{org}}$ . To identify a general way to

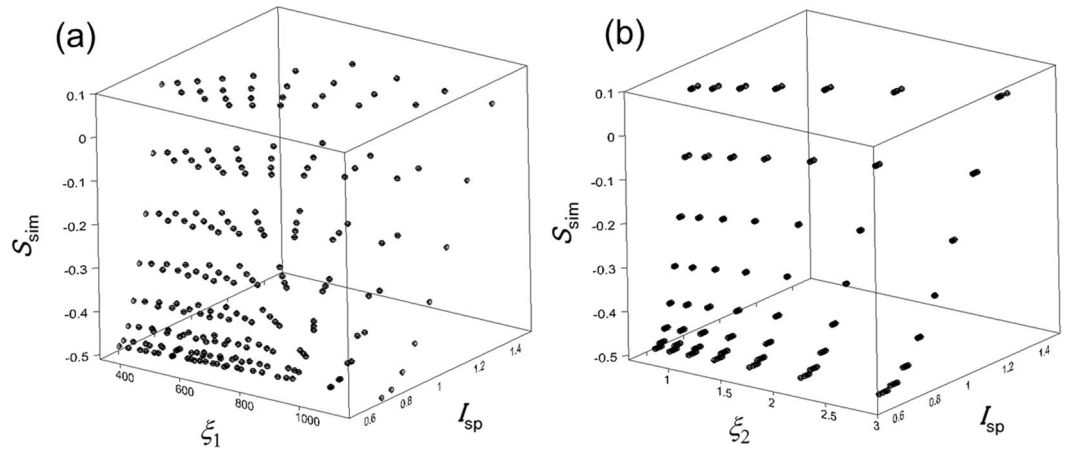


**Figure 2.** Simulated results of  $S_{sim}$  obtained by  $I_{sp}$  and (a)  $\xi_1$  or (b)  $\xi_2$ .

correlate these values, we applied the following strategy: (i) the parameter  $\xi$  is defined by the values of  $\lambda$ ,  $n_{air}$  and  $n_{org}$ . (ii) We considered a three-dimensional space defined by  $S_{sim}$ ,  $I_{sp}$ , and  $\xi$ . The definition of  $\xi$  was modified so that the simulated plots featured a smooth surface in  $S_{sim} - I_{sp} - \xi$  space. (iii) For various values of  $d$  and  $n_{sub}$  we found an equation describing the smooth surface, which correlated  $S_{sim}$  with  $I_{sp}$  and  $\xi$ . We used this equation to define the calculated  $S$  ( $S_{calc}$ ). For practical purposes,  $S_{calc}$  can be calculated from the equation from the experimentally obtained  $I_{sp}$  and a parameter set, which is defined by  $d$ ,  $\lambda$ ,  $n_{sub}$ ,  $n_{air}$  and  $n_{org}$ .

In step (i), to find an appropriate  $\xi$ , which created a smooth surface in  $S_{sim} - I_{sp} - \xi$  space, we arbitrarily considered the formula  $\xi_1 = \lambda / (n_{org} - n_{air})$  as an initial example. We defined  $\xi_1$ , in this way because it is plausible that the beam propagation may correlate with a wave vector. Figure 2a shows scatter plots in the  $S_{sim} - I_{sp} - \xi_1$  space, which were obtained from a simulation with  $d = 20$  nm and  $n_{sub} = 1.524$ . We set  $S_{sim}$  as the z axis, because  $S_{calc}$  becomes the desired calculation result in the practical use of the proposed method. As shown in Fig. 2a,  $\xi_1$  did not converge to create a smooth, indicating that  $\xi_1$  is not an appropriate parameter for calculation of  $S_{calc}$ . Thus, we modified the definition of  $\xi$  to achieve well-organized scattered plots as step (ii). When we tested a new parameter  $\xi_2$ , the scattered plots were well organized as shown in Fig. 2b.  $\xi_2$  is given by equation 1,

$$\xi_2 = [(n_{org} - n_{air})]^{-2}. \tag{1}$$

The plots in  $S_{sim} - I_{sp} - \xi_2$  space were insensitive to variation of  $\lambda$ . Four dots for 400, 500, 600, and 700 nm appeared at almost the same coordinates in Fig. 2b. This was because  $d$  is much smaller than  $\lambda$  and the effect of  $\lambda$  on the  $S_{sim} - I_{sp} - \xi_2$  plots was negligible unless a much thicker film ( $d \gg 20$  nm) was used.

Next, in step (iii), we derived an equation expressing the  $S_{calc}$  surface. To simplify the derivation, we first correlated the plots in the  $S_{sim} - I_{sp}$  plane, and then extended these to correlate the  $S_{sim} - I_{sp}$  relation with  $\xi_2$ . Figure 3 shows the  $S_{sim} - I_{sp}$  characteristics, which represent the  $S_{sim} - I_{sp} - \xi_2$  plots (Fig. 2b) viewed from the  $S_{sim} - I_{sp}$  plane. Each curve showed a sigmoid-like curve. Thus, we fitted the plots with a sigmoidal function, given by equation 2:

$$S_{calc, I_{sp}, \xi_2, d, n_{sub}} = b_{\xi_2, d, n_{sub}} + \frac{m_{\xi_2, d, n_{sub}}}{1 + \exp\left(\left\{h_{\xi_2, d, n_{sub}} - I_{sp}\right\} / r_{\xi_2, d, n_{sub}}\right)}, \tag{2}$$

where,  $b$  is the baseline of the  $S_{calc} - I_{sp}$  characteristics,  $m$  is the maximum value of the sigmoidal curve,  $h$  is the specific  $I_{sp}$  value when  $S_{calc} = h/2$ , and  $r$  is the inverse rate of increase of  $S_{calc}$  versus  $I_{sp}$ . Each plot of  $S_{sim}$  was reproduced well by eq. 2, demonstrating that the  $S_{calc} - I_{sp}$  relation could form the basis of an equation to reproduce the  $S_{sim} - I_{sp} - \xi_2$  surface. Next, we investigated the correlation of  $b$ ,  $m$ ,  $h$ , and  $r$  with  $\xi_2$ . The purpose of this operation was to correlate the  $S_{calc} - I_{sp}$  relation with  $\xi_2$ ; this is equivalent to looking down the three-dimensional  $S_{sim} - I_{sp} - \xi_2$  space from the  $I_{sp} - \xi_2$  plane (Fig. 2b). Figures 4a–d show the dependences of  $b$ ,  $m$ ,  $h$ , and  $r$  on  $\xi_2$ . The variables  $b$ ,  $m$ ,  $h$ , and  $r$  all exhibited clear dependences on  $\xi_2$ . The shapes of the curves suggested an exponential function, hence we fitted these with equations 3–6,

$$b_{\xi_2, d, n_{sub}} = a_{d, n_{sub}} \exp\left[-k_{d, n_{sub}} \left\{\xi_2 - c_{d, n_{sub}}\right\}\right] + e_{d, n_{sub}}, \tag{3}$$

$$m_{\xi_2, d, n_{sub}} = a'_{d, n_{sub}} \left(1 - \exp\left[-k'_{d, n_{sub}} \left\{\xi_2 - c'_{d, n_{sub}}\right\}\right]\right) + e'_{d, n_{sub}}, \tag{4}$$

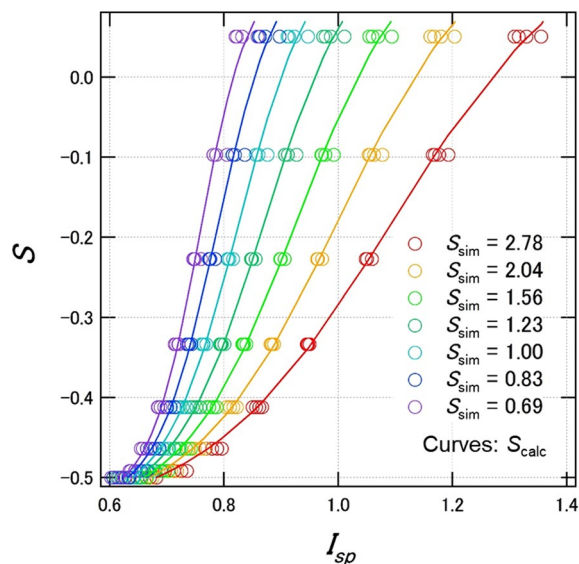


**Figure 3.**  $S - I_{sp}$  characteristics at  $d = 20$  nm and  $n_{sub} = 1.524$ . Dots indicate  $S_{sim}$ , i.e., a representation of the  $S_{sim} - I_{sp} - \xi_2$  plots (Fig. 2b) viewed from the  $S - I_{sp}$  plane. The sigmoidal curves show fitting results of  $S_{calc}$  (eq. 1).

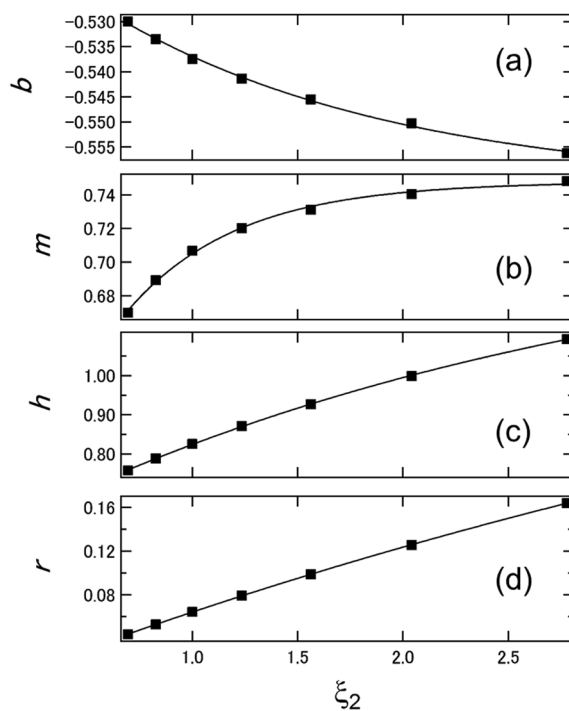


**Figure 4.** (a)  $b$ , (b)  $m$  (c)  $h$ , and (d)  $r$  as a function of  $\xi_2$ . The characteristics were obtained at  $d = 20$  nm and  $n_{sub} = 1.524$ .

$$h_{\xi_2, d, n_{sub}} = a''_{d, n_{sub}} \left( 1 - \exp \left[ -k''_{d, n_{sub}} \left\{ \xi_2 - c''_{d, n_{sub}} \right\} \right] \right) + e''_{d, n_{sub}} \tag{5}$$

$$r_{\xi_2, d, n_{sub}} = a'''_{d, n_{sub}} \left( 1 - \exp \left[ -k'''_{d, n_{sub}} \left\{ \xi_2 - c'''_{d, n_{sub}} \right\} \right] \right) + e'''_{d, n_{sub}} \tag{6}$$

Substrate	Glass ( $n_{\text{sub}} = 1.524$ )			Fused silica ( $n_{\text{sub}} = 1.460$ )		
	10	15	20	10	15	20
$a$	0.098604	0.110944	0.042013	0.197569	0.156029	0.11373
$k$	0.690732	0.178521	0.736613	0.96795	0.792135	0.397617
$c$	-1.18994	-2.72364	0.345428	-1.21634	-1.50049	-1.82734
$e$	-0.56855	-0.601617	-0.56287	-0.567663	-0.565258	-0.575086
$a'$	0.366794	0.36543	0.359072	0.372707	0.367789	0.360643
$k'$	17.1356	0.275624	1.90403	4.92218	2.34445	1.40428
$c'$	0.543513	-10.8917	-0.117778	0.228131	-0.464428	-0.358297
$e'$	0.400497	0.405369	0.388698	0.397003	0.394126	0.39185
$a''$	0.644241	0.706328	0.689067	0.597502	0.618666	0.679183
$k''$	0.356334	0.307937	0.345435	0.334855	0.330799	0.298034
$c''$	0.441737	0.582837	0.526038	0.702383	0.737254	0.76181
$e''$	0.72579	0.746449	0.720144	0.722417	0.719095	0.719382
$a'''$	0.328729	0.192264	0.393989	0.194786	0.221476	0.2802
$k'''$	0.177307	0.165193	0.159079	0.159687	0.147584	0.125966
$c'''$	1.23618	5.02439	1.17711	5.11488	5.16589	5.29678
$e'''$	0.071262	0.243959	0.0754636	0.236137	0.248144	0.264477
Max. error of $S_{\text{calc}}$	0.076 <sup>a</sup>	0.048 <sup>a</sup>	0.111 <sup>a</sup>	0.067 <sup>a</sup>	0.034 <sup>a</sup>	0.064 <sup>a</sup>
	(0.021) <sup>b</sup>	(0.020) <sup>b</sup>	(0.040) <sup>b</sup>	(0.020) <sup>b</sup>	(0.016) <sup>b</sup>	(0.039) <sup>b</sup>

**Table 1.** All parameters for  $S_{\text{calc}}$  and their error from  $S_{\text{sim}}$ . <sup>a</sup> $1.6 \leq n_{\text{org}} \leq 2.2$ , <sup>b</sup> $1.6 \leq n_{\text{org}} \leq 2.0$ .

where,  $a, a', a'', a''', k, k', k'', k''', c, c', c'', c''', e, e', e'', e'''$ , and  $e''''$  are constants characterizing the  $b - \xi_2$ ,  $m - \xi_2$ ,  $h - \xi_2$ , and  $r - \xi_2$  curves. As shown in Fig. 4a–d, good fits were obtained with eqs 3–6. Hence the  $S$  values were arbitrarily calculated with eqs 2–6 based on these parameters. Table 1 summarizes all the parameters that we used to calculate the  $S_{\text{calc}} - I_{\text{sp}} - \xi_2$  surface, as shown in Fig. 5a. Here, we used  $d = 20$  nm and  $n_{\text{sub}} = 1.524$  (glass substrate). A surface plot was generated over the scattered  $S_{\text{sim}} - I_{\text{sp}} - \xi_2$  dots (Fig. 2b) to allow comparison. As shown in Fig. 5a, the calculated surface closely followed the simulated dots. To verify the reproducibility of our calculation compared with optical simulations,  $S_{\text{calc}} - S_{\text{sim}}$  was evaluated. This result is shown in Fig. 5b. The interpolated surface in the figure was generated by the spline approximation. In the ranges of  $0.69 \leq \xi_2 \leq 2.78$  and  $0.618 \leq I_{\text{sp}} \leq 1.32$ , the error was less than 0.111 at  $(\xi_2, I_{\text{sp}}) = (0.69, 0.746)$ . Furthermore, in the typical range of experimental conditions  $1.6 \leq n_{\text{org}} \leq 2.0$ , which corresponds to  $1.99 \leq \xi_2 \leq 2.78$ , the error was less than 0.040. The error comes mainly from the scattered  $S_{\text{sim}}$  values, which depend on  $\lambda$ . As mentioned earlier, the effect of  $\lambda$  on the  $S_{\text{sim}} - I_{\text{sp}} - \xi_2$  plots was negligible, but only small scattering was included. Here, it should be noted that the scale of the error can be considered very small for the practical use. Thus, we conclude that our method is of potential use in the direct calculation of  $S_{\text{calc}}$  from experimental angular dependent PL measurements.

We could develop the method for calculating  $S_{\text{calc}}$  from the parameters  $\xi_2$  and  $I_{\text{sp}}$ . However, here we should note that the parameters  $a, a', a'', a''', k, k', k'', k''', c, c', c'', c''', e, e', e'', e'''$ , and  $e''''$  were dependent on  $n_{\text{sub}}$  and  $d$ , meaning that the scope of this calculation method is limited by  $n_{\text{sub}}$  and  $d$ . However, both  $n_{\text{sub}}$  and  $d$  are predetermined by the sample preparation. Therefore, this limitation does not greatly influence the practical applicability of this approach to calculations. Glass ( $n_{\text{sub}} = 1.524$ ) and fused silica ( $n_{\text{sub}} = 1.460$ ) substrates are often used in angular dependent PL measurements, hence parameters for both substrates are listed in Table 1. Owing to the variation of  $d$ , the parameters for  $d = 10, 15, 20$  nm are also independently listed in Table 1. One would consider whether the dipole orientation in such an ultra-thin film can be preserved in much thicker films. This is the case that one should carefully estimate the difference in the dipole orientations between the ultra-thin and thick films, especially for films as thick as 100 nm. Meanwhile, in the case of several tens of nm, it has been reported so far that the estimated orientation can be utilized to expect EL light outcoupling<sup>7,14,15</sup>. Thus, even in ultra-thin films, the estimated orientation can be used for considering the optical effect in practical devices. As shown in Fig. 6, the shape of the  $S_{\text{calc}}$  surface depends on  $d$ . The differences among the  $S_{\text{calc}}$  surfaces was very small, but significant. From a technical viewpoint, reliably adjusting the value of  $d$  on a nanometre scale is difficult to achieve experimentally (e.g., through vacuum vapour deposition). If  $d$  is not defined with sufficient accuracy, its value may be confirmed by an annealing treatment of the film above a temperature where the molecular configuration of the host matrix becomes disordered (this temperature often coincides with the material's glass transition temperature)<sup>7</sup>. After annealing,  $S_{\text{calc}}$  should become zero. Thus, one can estimate  $d$ , and determine the appropriate  $S_{\text{calc}}$  surface from the crossing point of the experimentally obtained  $I_{\text{sp}}$  and  $\xi_2$  where  $S_{\text{calc}} = 0$ .

To test the validity of the calculation method, we calculated  $S$  values based on previous publications and compared our  $S_{\text{calc}}$  with the reported  $S$  values, which were obtained by photonic mode density simulations. This validation is equivalent to a comparison between our calculation method of  $S_{\text{calc}}$  and the optical simulation. We selected TADF emitters doped into conventional host matrices, because TADF molecules have been reported to show a wide range of  $S$  values from  $-0.50$  to  $0.05$ . The binary molecular systems used were 10-[4-(4,6-diphenyl-1,3,5-triazin-2-yl)phenyl]-10*H*-phenoxazine (PXZ-TRZ); 3,3-di(9*H*-carbazol-9-yl)biphenyl (mCBP); 2,6-bis(4-(10*H*phenoxazin-10-yl)phenyl)benzo[1,2-*d*:5,4-*d'*] bis(oxazole) (*cis*-BOX 2); 4,4'-bis(*N*-carbazolyl)-1,1'-biphenyl (CBP), and 9-[4-(4,6-diphenyl-1,3,5-triazin-2-yl)phenyl]-*N*3,*N*3,*N*6,*N*6-tetraphenyl-9*H*-carbazole-3,6-diamine



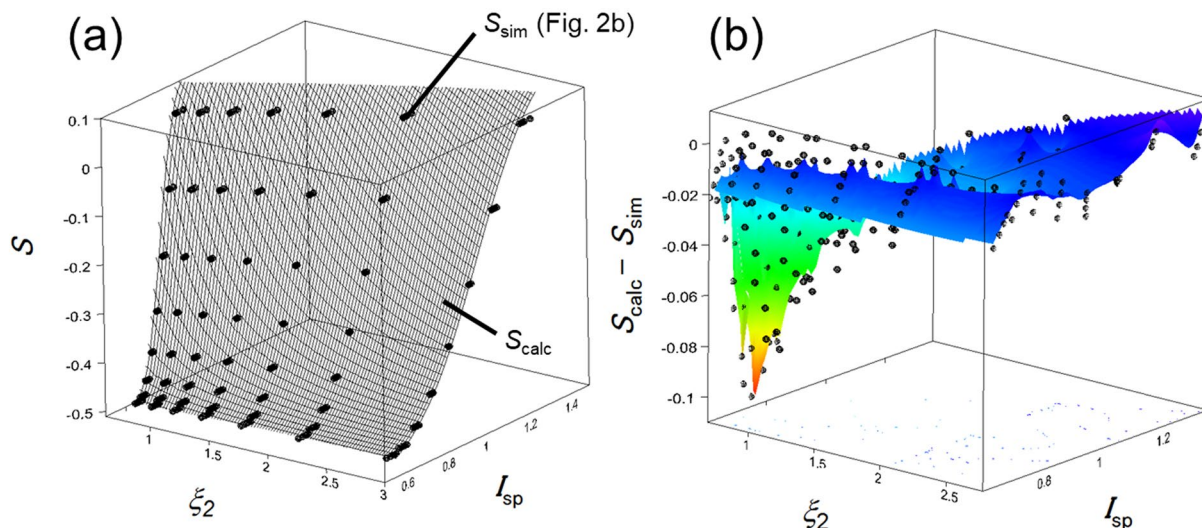


**Figure 5.** (a)  $S_{\text{calc}} - I_{\text{sp}} - \xi_2$  (surface) and  $S_{\text{sim}} - I_{\text{sp}} - \xi_2$  (dots) characteristics from the conditions  $d = 20$  nm and  $n_{\text{sub}} = 1.524$ . The  $S_{\text{calc}} - I_{\text{sp}} - \xi_2$  surface closely replicated  $S_{\text{sim}} - I_{\text{sp}} - \xi_2$  characteristics, suggesting that the  $S_{\text{calc}} - I_{\text{sp}} - \xi_2$  characteristics can be used to calculate  $S_{\text{calc}}$  at an arbitrary condition defined by  $I_{\text{sp}}$ ,  $d$ ,  $\lambda$ ,  $n_{\text{sub}}$ ,  $n_{\text{air}}$  and  $n_{\text{org}}$ ; the substrate should be glass or fused silica. (b) Error between  $S_{\text{calc}}$  and  $S_{\text{sim}}$  for each value of  $\xi_2$  and  $I_{\text{sp}}$  at  $d = 20$  nm and  $n_{\text{sub}} = 1.524$  (see Table 1).

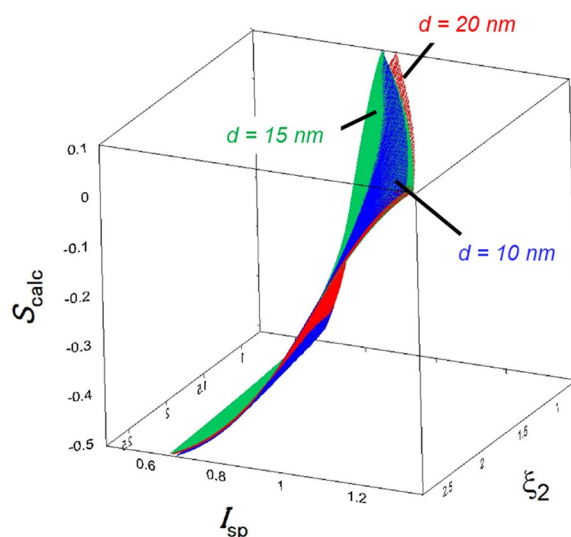


**Figure 6.** Variation of the  $S_{\text{calc}} - I_{\text{sp}} - \xi_2$  surfaces for  $d = 10, 15,$  and  $20$  nm, calculated with  $n_{\text{sub}} = 1.524$  (for a glass substrate).

(DACT-II):CBP. Table 2 summarizes the  $S_{\text{calc}}$  and reported  $S$  values. Even for the largest error, the differences between the calculated and simulated values were less than 0.05, and in good agreement with our estimation (Fig. 5b).

While the dipole orientation of a guest emitter doped in a host matrix has been evaluated by a combination of angular dependent PL measurements with optical simulation analysis, we developed the method to directly analyse a radiation pattern obtained in angular dependent PL measurements without the use of any optical simulations. The parameters used to evaluate the dipole orientation were  $a, a', a'', a''', k, k', k'', k''', c, c', c'', c''', e, e', e'', e'''$ , which were determined by  $d$  and the substrate type. For practical use of this method, we have listed parameters for typical glass and fused silica substrates with a range of  $d$  values from 10 to 20 nm. The considered range of  $d$  is sufficiently small to be able to neglect the effects of  $\lambda$  in the visible range (400–700 nm), hence one can use this method without considering  $\lambda$ . For practical applications, a radiation pattern should be measured and the value of  $n_{\text{org}}$  determined. When we applied this calculation method to estimate  $S_{\text{calc}}$  for previously reported results from TADF emitters, the resultant  $S_{\text{calc}}$  values reproduced the reported values well with an error of less than 0.05. The error was consistent with our estimated error, which was evaluated by a comparison of  $S_{\text{calc}}$

Sample	$\lambda/\text{nm}$	$d/\text{nm}$	$n_{\text{sub}}$	$n_{\text{org}}$	$S_{\text{calc}}$	$S$ (reported)	Difference	Reference
PXZ-TRZ:mCBP <sup>a</sup>	530	15	1.524	1.74	0.048	0.05	0.002	14
PXZ-TRZ:mCBP <sup>b</sup>	530			1.74	-0.142	-0.12	0.022	14
PXZ-TRZ:mCBP <sup>c</sup>	530			1.73	-0.357	-0.31	0.047	14
Cis-BOx2:CBP <sup>a</sup>	510			1.76	-0.452	-0.41	0.042	7
Cis-BOx2:CBP <sup>c</sup>	510			1.75	-0.518	-0.5	0.018	7
DACT-II:CBP	515			1.46	1.76	-0.339	-0.29	0.049

**Table 2.** Comparison of  $S_{\text{calc}}$  and reported  $S$  values. Vapour deposition at <sup>a</sup>300 K, <sup>b</sup>250 K, and <sup>c</sup>200 K.

with  $S_{\text{sim}}$  (Table 1). These results indicate that our calculation method is of potential use for practical estimations of dipole orientation.

This calculation method may not be suitable for all purposes, and if one is able to perform a full optical simulation, this would be the preferred way to analyse the data. However, this method shows potential for many diverse applications across research fields, in cases where the experimenter may not have experience in performing optical simulations. Dipole orientation is an important characteristic affecting photonic, electronic, excitonic, and optic properties of organic guest-host systems. This method may help researchers to rapidly calculated dipole orientations not only in OLED materials but many other binary molecular systems.

## Methods

**Optical Simulation.** The radiation pattern was calculated by a photonic mode density simulation using a commercial software package (setfos 3.4, Fluxim Co.). In the calculation, the far-field emission intensity of the substrate material as a function of  $\theta$  was simulated.  $\theta$  was varied from  $0^\circ$  to  $89^\circ$  in steps of  $1^\circ$ . A light-emitting layer with a thickness  $d$  of 10, 15, or 20 nm was placed in-between the substrate and an air layer of infinite thicknesses. The refractive index of the substrate ( $n_{\text{sub}}$ ) was set to be either 1.524 for an ordinary glass or 1.460 for fused silica, while that for air ( $n_{\text{air}}$ ) was 1.000. The refractive index of the substrate of the organic light-emitting layer ( $n_{\text{org}}$ ) was varied from 1.600 to 2.200 in steps of 0.100. For practical purposes this refractive index value can be considered to be equivalent to that of the host matrix unless  $n_{\text{org}}$  is strongly influenced by the guest molecules. The extinction coefficients of all materials were assumed to be zero. The emission wavelength  $\lambda$  was varied in the range 400–700 nm in steps of 100 nm. An emitting dipole was placed at the centre of the light emitting layer, and the dipole orientation  $\Theta_v$  was varied from 0 to 0.35 in steps of 0.05. Note that the simulation software uses  $\Theta_v$  as the variable parameter, thus we translated  $\Theta_v$  to  $S_{\text{sim}}$  for our analysis. The range of variation in  $\Theta_v$  corresponded to  $S_{\text{sim}}$  of  $-0.50$ – $0.05$ , meaning that the estimated dipole orientation completely covered the range from a horizontal orientation ( $S_{\text{sim}} = -0.5$ ) to complete disorder ( $S_{\text{sim}} = 0$ ). Although  $S_{\text{sim}} = 0.05$  indicates a slight vertical orientation, previous studies have shown that such an orientation is feasible. We neglected the  $S_{\text{sim}}$  range from 0.05 to 1.00, because this degree of orientations can be considered outside of the range obtainable by conventional deposition methods.

## References

- Yokoyama, D. Molecular Orientation in Small-Molecule Organic Light-Emitting Diodes. *J. Mater. Chem.* **21**, 19187–19202 (2011).
- Frischeisen, J., Yokoyama, D., Adachi, C. & Brütting, W. Determination of Molecular Dipole Orientation in Doped Fluorescent Organic Thin Films by Photoluminescence Measurements. *Appl. Phys. Lett.* **96**, 073302 (2010).
- Flämmich, M. *et al.* Oriented Phosphorescent Emitters Boost OLED Efficiency. *Org. Electron.* **12**, 1663–1668 (2011).
- Brütting, W., Frischeisen, J., Schmidt, T. D., Scholz, B. J. & Mayr, C. Device efficiency of organic light-emitting diodes: Progress by improved light outcoupling. *Phys. Status Solidi A* **210**, 44–66 (2013).
- Lin, T.-A. *et al.* Sky-Blue Organic Light Emitting Diode with 37% External Quantum Efficiency Using Thermally Activated Delayed Fluorescence from Spiroacridine-Triazine Hybrid. *Adv. Mater.* **28**, 6976–6983 (2016).
- Sun, J. W. *et al.* A Fluorescent Organic Light-Emitting Diode with 30% External Quantum Efficiency. *Adv. Mater.* **26**, 5684–5688 (2014).
- Komino, T. *et al.* Electroluminescence from Completely Horizontally Oriented Dye Molecules. *Appl. Phys. Lett.* **108**, 241106 (2016).
- Uoyama, H., Gouhi, K., Shizu, K., Nomura, H. & Adachi, C. Highly Efficient Organic Light-Emitting Diodes from Delayed Fluorescence. *Nature*. **492**, 234 (2012).
- Tao, Y. *et al.* Thermally Activated Delayed Fluorescence Materials Towards the Breakthrough of Organicelectronics. *Adv. Mater.* **26**, 7931–7958 (2014).
- Yang, Z. *et al.* Recent Advances in Organic Thermally Activated Delayed Fluorescence Materials. *Chem. Soc. Rev.* **46**, 915–1016 (2017).
- Schmidt, T. D. *et al.* Evidence for Non-Isotropic Emitter Orientation in a Red Phosphorescent Organic Light-Emitting Diode and its Implications for Determining the Emitter's Radiative Quantum Efficiency. *Appl. Phys. Lett.* **99**, 163302 (2011).
- Jurow, M. J. *et al.* Understanding and Predicting the Orientation of Heteroleptic Phosphors in Organic Light-Emitting Materials. *Nat. Mater.* **15**, 85–91 (2016).
- Kim, S.-Y. *et al.* Organic Light-Emitting Diodes with 30% External Quantum Efficiency Based on a Horizontally Oriented Emitter. *Adv. Funct. Mater.* **23**, 3896–3900 (2013).
- Komino, T., Tanaka, H. & Adachi, C. Selectively Controlled Orientational Order in Linear-Shaped Thermally Activated Delayed Fluorescent Dopants. *Chem. Mater.* **26**, 3665–2671 (2014).
- Kaji, H. *et al.* Purely Organic Electroluminescent Material Realizing 100% Conversion from Electricity to Light. *Nat. Commun.* **6**, 8476 (2015).

## Acknowledgements

This work was supported by JST ERATO Grant Number JPMJER1305, Japan, and the International Institute for Carbon Neutral Energy Research (WPI-I2CNER) sponsored by the Ministry of Education, Culture, Sports, Science, and Technology. T.K. thanks JSPS KAKENHI Grant Number 16K17972 and Mr. Kiyotada Hosokawa, Mr. Shigeru Eura, Dr. Kenichiro Ikemura, and Mr. Hirohiko Watanabe (Hamamatsu Photonics) for their early contributions and recognition of the possibility of a relationship between  $I_{sp}$  and S.

## Author Contributions

T.K. performed the optical simulations and calculations. T.K. and C.A. wrote the paper. T. K., Y.O., and C.A. planned the project, and Y.O. and C.A. supervised the project.

## Additional Information

**Competing Interests:** The authors declare that they have no competing interests.

**Publisher's note:** Springer Nature remains neutral with regard to jurisdictional claims in published maps and institutional affiliations.



**Open Access** This article is licensed under a Creative Commons Attribution 4.0 International License, which permits use, sharing, adaptation, distribution and reproduction in any medium or format, as long as you give appropriate credit to the original author(s) and the source, provide a link to the Creative Commons license, and indicate if changes were made. The images or other third party material in this article are included in the article's Creative Commons license, unless indicated otherwise in a credit line to the material. If material is not included in the article's Creative Commons license and your intended use is not permitted by statutory regulation or exceeds the permitted use, you will need to obtain permission directly from the copyright holder. To view a copy of this license, visit <http://creativecommons.org/licenses/by/4.0/>.

© The Author(s) 2017